CHEMISTRY
A European Journal

A Journal of
ChemPubSoc Europe

Accepted Article

Title: Highly efficient photocatalytic degradation of dyes by a novel copper-triazolate metal-organic framework

Authors: Guang Yang, Chen-Xia Liu, Wen-Hua Zhang, Nan Wang, Penghu Guo, Martin Muhler, Yuemin Wang, Zhongfang Chen, and Shiru Lin

To be cited as: *Chem. Eur. J.* 10.1002/chem.201803306

Link to VoR: http://dx.doi.org/10.1002/chem.201803306

Supported by
ACES

WILEY-VCH

10.1002/chem.201803306

WILEY-VCH

Highly efficient photocatalytic degradation of dyes by a novel copper-triazolate metal-organic framework

Chen-Xia Liu,[a] Wen-Hua Zhang,[a] Nan Wang,[a] Penghu Guo,[b] Martin Muhler,[b, c] Yuemin Wang,[d] Shiru Lin,[e] Zhongfang Chen,[e] Guang Yang *[a]

Abstract: A novel Cu^{I} 3,5-diphenyltriazolate metal-organic framework (CuTz-1) was synthesized and extensively characterized by a multi-technique approach. The combined results provided solid evidence that CuTz-1 features unprecedented Cu_5tz_6 cluster as SBU with channels of *ca* 8.3 Å diameter. This MOF material, which is both thermally and chemically (basic and acidic) stable, exhibits semi-conductivity and high photocatalytic activity towards degradation of dyes in the presence of H_2O_2. Its catalytic performance is superior to that of reported MOFs and comparable to some composites, which has been attributed to high efficiency of generating •OH – the most active species for degradation of dyes. It is suggested that the photogenerated holes are trapped by Cu^{I} yielding Cu^{II}, the latter of which behaves as a catalyst for a Fenton-like reaction to produce extra amount of •OH in addition to that formed *via* scavenging of photogenerated electrons by H_2O_2. Furthermore, it has been shown that a dye-mixture (methyl orange, methyl blue, methylene blue and rhodamine B) can be totally decolorized by using CuTz-1 as photocatalyst in the presence of H_2O_2 under the irradiation of a Xe lamp or *natural sunlight.*

Introduction

Dye-containing wastewater, largely discharged from textile, paper or printing industries, is one of the main sources of water pollution.[1, 2] The treatment of dye-containing wastewater presents a tremendous challenge for human beings not only because of the still rapidly growing discharge amount, but also due to the stable structures of dye molecules (usually conjugated), which render them chemical inert to light, heat and oxidizing agents, and therefore make it rather difficult to decompose or degrade dyes.[3] Although a number of methods, such as adsorption, biodegradation, chemical oxidation, coagulation, flocculation, *etc.*,[4-7] have been used for the treatment of dyes, new materials and technologies,[8] with high efficiency, wide applicability, economic feasibility and simplicity of design/operation, are still urgently demanded in order to better cope with this increasingly serious pollution issue, especially in some developing countries.

[a] C.-X. Liu, Dr. W.-H. Zhang, N. Wang, Prof. Dr. G. Yang
College of Chemistry and Molecular Engineering
Zhengzhou University, 450001 Zhengzhou, China
E-mail: yang@zzu.edu.cn
[b] P. Guo, Prof. Dr. M. Muhler
Laboratory of Industrial Chemistry
Ruhr-University Bochum, 44780 Bochum, Germany
[c] Prof. Dr. M. Muhler
Max Planck Institute for Chemical Energy Conversion
45470 Mülheim an der Ruhr, Germany
[d] Dr. Y. Wang.
Institute of Functional Interfaces (IFG)
Karlsruhe Institute of Technology (KIT), 76344 Eggenstein-Leopoldshafen, Germany
[e] S. Lin, Prof. Dr. Z. Chen
Department of Chemistry, University of Puerto Rico
Rio Piedras, San Juan, PR 00931, USA

Metal-organic frameworks (MOFs), developed from coordination compounds since about two decades ago, have been recently gaining more and more attention in materials science.[9-13] As a novel emerging type of materials, the structures of MOFs can be, at least in part, designed, prepared and modified for a given purpose not only due to the well-established construction theory and assembling strategies for MOF synthesis, but also because of the seemingly infinite number of choices for the two components of MOFs – metal ions (clusters) and organic linkers.[14-16]

Adsorptive removal of dyes is regarded as one of the competitive methods because of its high efficiency and easy operation.[17, 18] Several reports appeared using MOFs as adsorbent to remove dyes from solutions, mostly *via* ion-exchange processes.[19-22] Due to the microporosity of MOFs, for larger dye molecules it was found to be difficult to enter the pores or inner voids of MOFs, thus resulting in a lower adsorption capacity. In addition, adsorption by MOFs *via* ion-exchange would experience charge selectivity, that is, only oppositely charged dye ions can be exchanged into the interior of a charged MOF structure. Although the size- and/or charge-selectivity are useful for the design of MOF-based adsorbents for a specific dye molecule, for the treatment of wastewater containing complex dye compositions these characteristics are usually unfavorable for the practical use of MOFs in this regard.

On the other hand, photocatalysis has drawn much attention worldwide in the elimination of contaminants in water, because it provides the possibility to employ sustainable and abundant solar energy to promote reactions under mild conditions.[23, 24] Semiconductors such as TiO_2,[25-27] other metal oxides[28] and metal sulfides[29] have been exploited as photocatalysts for the purpose of catalytic decomposition /decolorization of dyes. The catalytic effectiveness of these semiconductors heavily relies on the photo-induced electrons and/or holes. It has been found that these catalysts usually suffer from limitations such as fast recombination of the electron-hole pairs, low solar energy utilization efficiency, and easy agglomeration.[30] Therefore, new catalytic materials showing high photocatalytic performance are desirable.

More recently MOFs have once again attracted academic interest in their potential use as a new type of photocatalyst.[30-33] Qiu *et al*. found that the efficient degradation of methylene blue (MLB) can be achieved under irradiation of UV or visible lights by using MIL-53(Fe) as photocatalyst.[34] Xing's group recently reported that NNU-36 is a highly efficient heterogeneous photocatalyst for the reduction of aqueous Cr^{VI} and degradation of dyes (rhodamine B: RhB, rhodamine 6G: R6G, MLB).[35] These research reports, together with others,[36-39] have revealed the enormous potential held by MOFs for their use in photocatalytic removal of environmental contaminants.

Inspired by our recent progress in the utilization of the silver 3,5-diphenyltriazolate MOF (previously designated as 1-NO_3 and here denoted as AgTz-1) in CO_2 uptake[40, 41] and Cr^{VI} removal,[42] we attempted to extend its application to the sorption of dye

molecules from aqueous solution. Preliminary test showed that AgTz-1 can efficiently adsorb methyl orange (MO, a smaller anionic dye) in water, however, for the other three dye molecules-methyl blue (MB, larger anionic), MLB (cationic), and RhB (cationic), this MOF failed to work as well as it for MO, indicative of the size- and charge-selectivity experienced for ion-exchange using MOF materials.

The coordination properties of Cu^{I} are similar to those of Ag^{I} in many cases, although copper is more prone to show Cu^{I}/Cu^{II} redox chemistry. It is therefore possible to prepare a Cu^{I}-containing MOF while the structure remains similar to that of AgTz-1. The former would show some new functions like redox activity, luminescence or catalytic activity and may find substantial use in the treatment of organic contaminants in wastewater. Here, we report the synthesis, characterization and structure of a new MOF based on Cu^{I} 3,5-diphenyltriazolate (denoted as CuTz-1), which is isostructural to our previously reported AgTz-1, but behaves differently from AgTz-1 in many of its physical and chemical properties. Photocatalytic performance and mechanism of CuTz-1 was investigated in detail for the degradation of dyes in aqueous solution.

Results and Discussion

Characterization and crystal structure of $Cu_8(3,5\text{-}Ph_2\text{-}tz)_6(HSO_4)_2\cdot(H_2O)_{5.5}$ (CuTz-1-HSO_4)

The colorless crystals of CuTz-1-HSO_4 were firstly prepared by a hydrothermal reaction of $Cu(NO_3)_2$ with 3,5-diphenyltriazole in dilute H_2SO_4 solution in 75% yield. Interestingly, Cu^{II} ions were reduced to Cu^{I} under hydrothermal conditions and triazole was deprotonated during the synthesis, although the reaction medium is acidic. Copper(II) perchlorate was also used as the metal source and the same MOF structure can be obtained with ClO_4^- as counter anion in a lower yield of 38%.

X-ray single crystal structure analysis shows that CuTz-1-HSO_4 crystallizes in the hexagonal space group - $P6_322$, and exhibits a 3D porous structure. Cationic skeleton $\{Cu_3[Cu_5(3,5\text{-}Ph_2\text{-}tz)_6]\}_n^{2+}$ is composed of the trigonal bipyramidal clusters - $[Cu_5(3,5\text{-}Ph_2\text{-}tz)_6]^-$ (Figure 1a), which are further connected through the linear coordination of Cu^{I}, forming a 3D metal-organic framework (MOF) structure (Figure 1b). In this structure, all the 3,5-diphenyltriazolate anions act as $\mu_3\text{-}N_{tz}^1,N_{tz}^2,N_{tz}^4$ bridging ligand. On the other hand, there are three crystallographically independent Cu^{I} ions which have different chemical environments: Cu1 is triply coordinated by N atoms forming a triangular CuN_3 arrangement, and is located at the apex of a Cu_5 cluster; Cu2 adopts a linearly coordination serving as the equatorial vertex of the Cu_5 cluster; the linearly coordinated Cu3 functions as a "linker" connecting two N_{tz}^4 atoms from a pair of adjacent clusters of $[Cu_5(3,5\text{-}Ph_2\text{-}tz)_6]^-$. Within the Cu_5 cluster, the distances of $Cu_{ax}\cdots Cu_{eq}$, $Cu_{ax}\cdots Cu_{ax}$, $Cu_{eq}\cdots Cu_{eq}$ are 3.130(1), 3.350(1), and 4.579(1) Å, respectively. Each Cu_5tz_6 cluster is connected with six peripheral identical clusters, in a trigonal prismatic arrangement, by six Cu3 atoms, and therefore functions as 6-connected trigonal prismatic secondary building units (SBU) in the structure of CuTz-1. If the Cu_5tz_6-SBU is regarded as a 6-connected node, the net underlying CuTz-1 is **acs** (or $4^9\cdot6^6$) (Figure 1c).[43] Extensive π-π interactions involving phenyl and triazolyl rings were observed in the crystal structure of CuTz-1, which may also contribute to the stabilization of the structure. (Figure S1)

Due to the severe thermal disorder, the anions and solvents cannot be definitely located in the Fourier map, however, the presence of two HSO_4^- anions is required by charge balance and was verified by elemental analysis and IR spectra. (Figure S2). PLATON calculation gives a porosity of 24.4% for the squeezed structure of CuTz-1, this value would be lower if the volume of anions were taken into consideration.

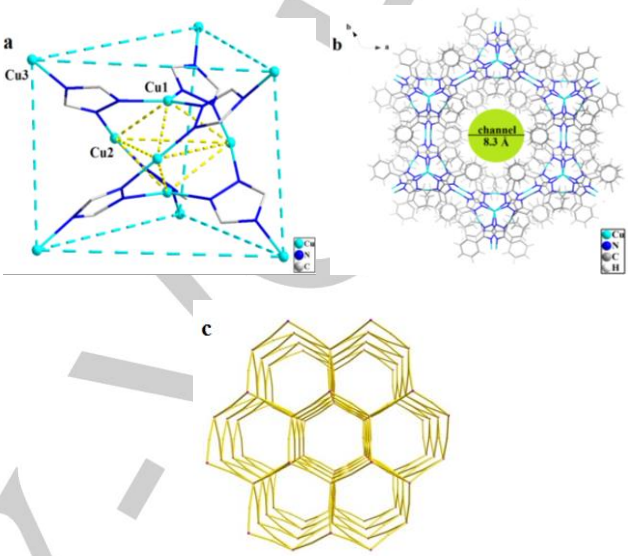

Figure 1. (a) The trigonal-prismatic $Cu_3[Cu_5(\mu_3\text{-}3,5\text{-}Ph_2\text{-}tz)_6]^{2+}$ repeating unit of the three-dimensional structure, Cu1-N, 1.977(2); Cu2-N, 1.868(2); Cu3-N, 1.876(2) Å; (b) Packing diagram of CuTz-1 viewed along the *c*-axis, showing one channel with diameter of *ca.* 8.3 Å (if the van der Waals' radius of H is taken into consideration, the effective diameter of the channels is estimated to be *ca* 6.0 Å); (c) The topological net underlying the structure of CuTz-1.

Synthesis and characterization of the powdery sample of CuTz-1

For the further properties investigation of this new MOF, a large quantity of the sample is needed. A facile, fast，energy-saving synthesis of this MOF is desired for further study, which was successfully achieved by simply mixing $Cu(CH_3CN)_4BF_4$ and triazole in degassed methanol. The chemical formula of the powdery sample was evaluated to be $Cu_8(3,5\text{-}Ph_2\text{-}tz)_6(BF_4)_2(CH_3OH)_3$ based on the result of CHN elemental analysis and IR spectroscopy. As shown in Figure S2a, there is a strong broad band at 3440 cm^{-1}, which can be assigned to the vibration of O-H. The weak peaks at 2926 cm^{-1} and 2853 cm^{-1} are possibly caused by the asymmetric and symmetric C-H vibrations of methanol molecules. The presence of BF_4^- (as counterion) was verified by its characteristic IR peak at 1084 cm^{-1} (Figure S2b). Moreover, the structure of the powdery sample is almost the same as that of CuTz-1-HSO_4, as evidenced by comparison of their PXRD patterns (Figure S3). The notation of CuTz-1-BF_4 was therefore coined for the powdery sample to show that both crystalline and powdery samples actually possess the same cationic MOF-skeleton and the main difference lies in their counterions. For the sake of convenience, we use an even more succinct notation – CuTz-1 for the powdery MOF in this paper.

The thermal stability of CuTz-1 was evaluated by thermogravimetric analysis. As shown in Figure S4, the TG

curve in air exhibits two weight loss steps. In the temperature range of 55 - 100 °C, the weight loss (4.22%) is attributed to the removal of methanol molecules (calculated value: 4.57%). The second severe weight loss observed between 335 - 800 °C is probably related to the decomposition of the framework. The final product, accounting for 31.75% of the total mass, is considered to be CuO according to the calculated residual weight percentage (32.50% as CuO).

In order to determine the pH stability of CuTz-1, the MOF samples were suspended in aqueous solutions at different pH for 24 h, followed by PXRD measurements to monitor the structural change of the MOF. As shown in Figure S5, the structure of CuTz-1 remains unchanged in the pH range of 3 - 11.

The luminescence spectra show that CuTz-1 exhibits a broad emission with maximum at 525 nm at room temperature when excited at 325 nm (Figure 2). The lifetime of this emission was measured to be 33 μs, indicative of phosphorescence. According to the previous studies on luminescent properties of Cu^{I} complexes, the low-energy emission can be assigned to ^{3}MLCT or ^{3}MM excited states. In the present case, the shortest Cu···Cu distance is 3.130(1) Å, which is slightly larger than the sum of van der Waals radius of the two copper atoms (2.80 Å).[44] It is thus conjectured that the emission originates from a triplet metal-to-ligand excited state transition (^{3}MLCT), possibly modified by weak Cu···Cu interactions.[45-51]

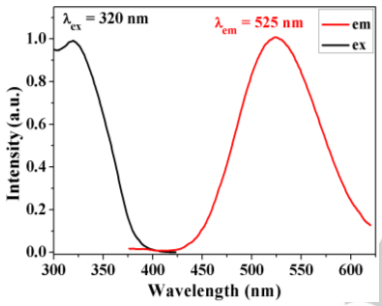

Figure 2. The photoluminescence spectrum of CuTz-1.

In order to probe the porosity of this MOF, nitrogen physisorption was conducted on CuTz-1 at 77 K. Prior to the measurement, the CuTz-1 sample was heated at 45 °C under high vacuum for 4h to remove residual methanol molecules. The N_2-adsorption/desorption isotherms obtained follow type I adsorption behavior,[52] revealing permanent microporosity of CuTz-1 (Figure 3). The BET surface area was determined to be 215.5 m^2 g^{-1}, and the pore size to approximately 0.64 nm,[53] which is in good agreement with the crystal structure data.

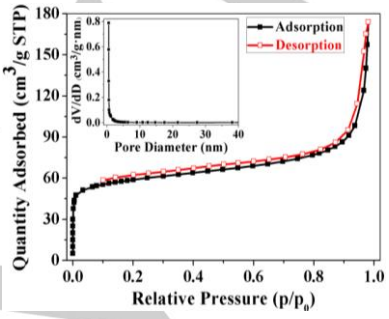

Figure 3. Nitrogen adsorption (black) and desorption (red) isotherms of CuTz-1 at 77K. Inset: Pore size distribution calculated from the isotherms.

Adsorption of organic dyes on AgTz-1 and CuTz-1

The adsorptive behavior of two MOFs was investigated for the removal of dyes from aqueous solution, and the results are listed in Figure 4 and Table S2. As can be seen, both MOFs can effectively remove smaller-sized anionic MO from water, however, the removal rate for other dyes is much lower under the same conditions: 35% for larger-sized anionic MB and less than 10% for cationic MLB and RhB.

IR spectra of the MO-adsorbed samples demonstrate the appearance of characteristic peaks of RSO_3^-, which is accompanied by a substantial attenuation of the peaks from original MOFs (1084 cm^{-1} for BF_4^- and 1384 cm^{-1} for NO_3^-) (Figure S6). These findings indicate the occurrence of an anion-exchange process, which we observed in Cr^{VI} removal by AgTz-1.[42]

The adsorption of MO by AgTz-1 and CuTz-1 is essentially an anion-exchange process between the anionic MO and the counter-ions within the cationic skeletons of $[M_8tz_6]_n^{2+}$. Since the dimension of MO is small enough to be trapped in the channels of the MOFs, the observed high removal rate for MO is thus not unexpected. It should be pointed out that the MOFs still retain their structures after MO-adsorption, as demonstrated by PXRD measurements (Figure S7).

On the other hand, MB, although anionic, has a much larger size than MO, which makes it impossible for MB to enter the inside of the MOF crystal. The much lower removal rate for MB is probably a result of surface adsorption. As for cationic RhB and MLB, it is not surprising to find that both MOFs (AgTz-1 and CuTz-1) failed to absorb them, because the cationic MOF skeletons cannot hold additional cations if the adsorption is based on anion exchange.

To summarize, MTz-1 MOFs can be used as a MO adsorbent, however, for the treatment of complex dye-mixtures, adsorptive removal by these MOFs suffers from the so-called “charge-selection” and “size-exclusion” effects, which thus limiting the wide applicability for this purpose.[20]

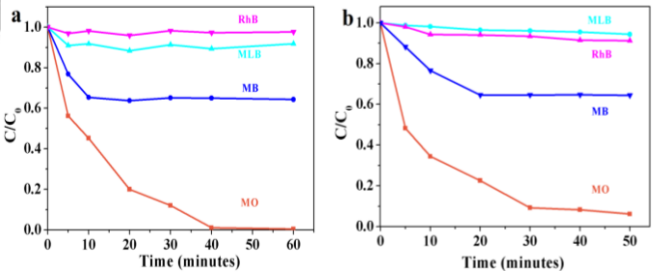

Figure 4. Percentages of dyes remaining in the aqueous solution monitored with time in the presence of (a) AgTz-1 and (b) CuTz-1 (MO: methyl orange; MB: methyl blue; MLB: methylene blue; RhB: rhodamine B).

Photocatalytic degradation of dyes by CuTz-1

Preliminary test revealed that CuTz-1 can decolorize the dye solutions in the presence of H_2O_2 under photoirradiation, while AgTz-1 is inactive for the photodegradation of dye molecules. A detailed investigation therefore ensued on the photocatalytic degradation of dyes by using CuTz-1 as photocatalyst. The four common dyes were chosen as representatives of different types of dyes (anionic: MO, MB; cationic: MLB, RhB; azo dye: MO; triarylmethane dye: MB; thiazine dye: MLB). To investigate the roles played by different

factors such as H_2O_2, CuTz-1 and photoirradiation, seven experimental conditions have been used for each dye: (1) H_2O_2/dark; (2) CuTz-1/dark; (3) H_2O_2/CuTz-1/dark; (4) blank (irradiation only); (5) H_2O_2/irradiation; (6) CuTz-1/irradiation; (7) H_2O_2/CuTz-1/irradiation. As shown in Figure 5, the best degradation result can only be achieved when H_2O_2, CuTz-1 and irradiation are applied simultaneously to the dye-containing system. For MO and MB, the observed removal of dye under CuTz-1/dark can be attributed mainly to the adsorption of the dyes within the channels or on the surface of MOF. We also noticed that the degradation performance of H_2O_2/CuTz-1/dark is always better than that of CuTz-1/dark for each dye under investigation. When irradiation is considered, we found that the irradiated groups exhibit more or less higher removal rate than the corresponding groups in the dark.

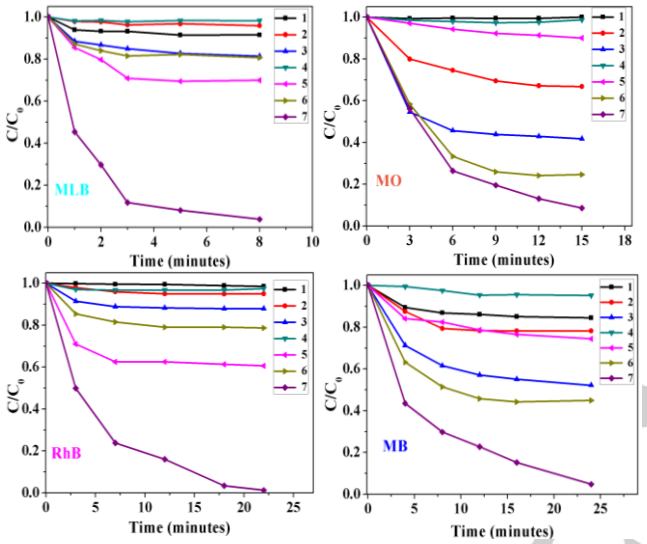

Figure 5. Degradation of dyes under different conditions. (1) H_2O_2/dark; (2) CuTz-1/dark; (3) H_2O_2/CuTz-1/dark; (4) blank (irradiation only); (5) H_2O_2/irradiation; (6) CuTz-1/irradiation; (7) H_2O_2/CuTz-1/irradiation (MO: methyl orange; MB: methyl blue; MLB: methylene blue; RhB: rhodamine B).

It is noticed that different dyes display different sensitivity to the degradation conditions used here: the time needed for complete removal of dyes is 8 min for MLB, 15 min for MO, 22 min for RhB and 24 min for MB (Figure S8). To facilitate the evaluation of the efficiency of the catalyst and the comparison with literature data, the concentration change of dye *vs.* time is simulated using a first-order kinetic model, which can be written as $\ln(C/C_0) = kt$. As shown in Figure S9-S12, the photodegradation of dyes over CuTz-1 follows first-order kinetics, and the rate constants (k) are 0.42 min^{-1}, 0.17 min^{-1}, 0.19 min^{-1} and 0.13 min^{-1} for MLB, MO, RhB and MB, respectively. From Table 1, one can clearly find that CuTz-1 exhibits high photocatalytic activity towards dyes in the presence of H_2O_2, its efficiency in this regard is higher than those of reported MOFs and other one-component materials such as nanoparticles, and comparable to those of composite materials. It should be pointed out that degradation data for methyl blue (MB) has not yet been reported in the literature, to the best of our knowledge.

Since the adsorption of dyes may affect the photocatalytic performance of MOFs, the degradation of MO and MB over CuTz-1 was conducted after the adsorption-desorption equilibrium was achieved. As shown in Figure S13 and Table 1, the rate constants k are 0.15 and 0.12 min^{-1} for MO and MB, respectively, slightly lower than those obtained before achieving the adsorption equilibrium.

In order to assess the reusability of CuTz-1, the photocatalytic degradation of each dye was run 4 cycles. As can be seen in Figure S14-S17, CuTz-1 still held similar photocatalytic efficiency even after being reused for 4 times. Importantly, the PXRD patterns of CuTz-1 after photo-degradation are almost the same as that of as-synthesized sample, confirming that the catalyst did not degrade under the photodegradation reaction condition. From comparison of SEM images (Figure S18), we noticed that the morphology of CuTz-1 did not change significantly much after 4 cycles reaction, although the surface of some crystals became coarse and shrank a little as seen in the SEM images of the recycled samples.

Table 1. Rate constants for photo-degradation of dyes by CuTz-1 in comparison with other reported catalysts.

Dye	Catalyst	k (min^{-1})	Ref.
MLB	MIL-53(Fe)	0.125	[34]
	NNU-36	0.0315	[35]
	UiO-66-NH_2	0.0071	[54]
	lp-2	0.01916	[55]
	12.5Cu@SBA-15	0.51	[56]
	RGO/Co DND nanocomposite	0.4627	[57]
	CuTz-1	**0.42**	This work
RhB	NNU-36	0.0468	[35]
	MIL-53(Fe)	0.0445	[58]
	MHMCs	0.0513	[58]
	RGO/Co DND nanocomposite	0.3367	[57]
	Porous Carbon- Fe_2O_3	0.2-0.14	[59]
	Bi(0.25%)/Co(0.25%)-TiO_2	0.00315	[60]
	Hollow Pt/Ag nanosphere	0.047	[61]
	CuTz-1	**0.19**	This work
MO	ZIF-8-600	0.0033	[62]
	ZIF-67-600	0.0025	[62]
	ZnO	0.0066	[62]
	Pt NP	0.0029	[63]
	Au NP	0.0049	[63]
	ZnO@C-N-Co	0.0283	[62]
	RGO/Co DND nanocomposite	0.2912	[57]
	CuTz-1	**0.17**	This work
		0.15 *	
MB	**CuTz-1**	**0.13**	This work
		0.12 *	

* Values were obtained after the adsorption-desorption equilibrium was achieved.

The degradation of mixed dyes (MLB, RhB, MO and MB) on CuTz-1 was also studied. CuTz-1(12 mg) and H_2O_2 (400 μL) were added into 20 mL of the aqueous solution of mixed dyes (the concentration of each dye is 12 mg/L). Figure 6 shows the UV-vis spectra for the photodegradation of MLB-MO-RhB-MB mixture on CuTz-1. Before degradation, the mixture had a dark brown color, resulting from the simultaneous presence of four dyes. Under Xe lamp irradiation, the mixture gradually faded from purple to colorless after 21 min, and the PXRD pattern of CuTz-1 after photodegradation remained the same as that of pristine MOF (Figure S19). This experiment demonstrates that CuTz-1 still retains its high catalytic efficiency for complex dye mixtures. In order to further evaluate the practicability of this catalyst, the degradation of mixed dyes was also conducted in the open air, the natural sunlight acting as the irradiation source.

It is found that the dyes were totally decolorized with 80 min when the natural sunlight was used instead of Xe lamp.

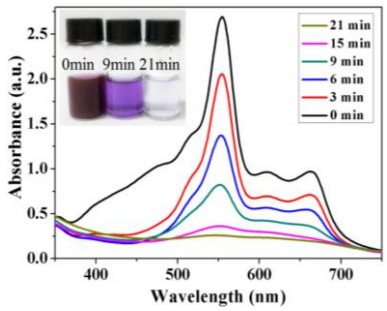

Figure 6. The UV-vis spectral changes of mixed dyes with time. Insert: Photographs of mixed dyes solutions taken at different time points of photocatalytic degradation reaction (mixed dyes: methyl orange, methyl blue, methylene blue and rhodamine B).

Photocatalytic mechanism

Semi-conductivity of CuTz-1

Since CuTz-1 shows high photocatalytic efficiency under Xe-lamp irradiation, it is hypothesized that this MOF may possess semi-conductivity. Some recent studies demonstrated that MOFs constructed by metals with variable valence exhibit semi-conductivity and act as photocatalyst.[64, 65] Thus, UV-vis DRS was conducted to evaluate the optical properties of the samples.

As shown in Figure 7, AgTz-1 has a strong broad absorption band in the range of 200 to 300 nm, the absorbance dropped sharply beyond 310 nm, resulting in nearly no absorption in the visible region. On the other hand, CuTz-1 shows a relatively weak absorption peak at 213 nm and two strong peaks at 267 nm and 300 nm in the UV region. Interestingly and importantly, the absorbance of CuTz-1 in the visible region still remains in high (about 3/5 that of highest peak) throughout the entire visible spectrum up to 800 nm.

The band gap of materials can be estimated from UV-vis DRS according to the Kubelka-Munk function. As shown in Figure S20, the band gap (E_g) is obtained as the intersection point between the energy axis and the line extrapolated from the linear portion of the adsorption edge in a plot of the Kubelka-Munk function *F* against *E*.[66, 67] The E_g values of CuTz-1 and AgTz-1 were determined to be 2.4 eV and 4.0 eV, respectively. Compared to AgTz-1, CuTz-1 has a much narrower energy gap and is expected to behave as a semiconductor. Theoretical calculation gave a band gap of 2.21 eV for CuTz-1, in reasonable agreement with our experimental results (see ESI for more calculation details).

It is noteworthy that CuTz-1 exhibits continuous strong absorption in the near infrared region (NIR) (Figure S21), which could be tentatively assigned to the intervalence charge-transfer bands (IVCT), and to a lesser extent, d-d transition.[68,69] As is known to all, IVCT is characteristic of mixed-valence complexes.[70] In the present case, the structure of CuTz-1 is undoubtedly based on Cu^{I}. Still and all, XPS analysis suggests that there is a tiny amount of Cu^{II} on the surface of CuTz-1 (see next part for details on XPS measurement). It is thus supposed that the absorption in NIR by CuTz-1 could be related to the IVCT band involving $Cu^{I} \rightarrow Cu^{II}$ within the polymeric structure. Further investigation is required to understand the nature of the unusual absorption behavior of CuTz-1.

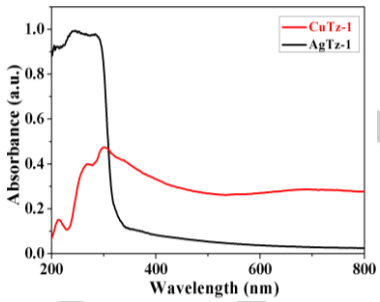

Figure 7. UV-vis absorption spectra of CuTz-1 and AgTz-1 at ambient temperature.

XPS analysis of the catalysts

We further conducted XPS measurements for as-synthesized and pretreated CuTz-1 catalysts in order to obtain more information about the chemical and electronic states of elements, as well as the atomic concentration of different species (Cu^{I}/Cu^{II}, O- and F- containing species) on the surface of the catalyst. The identification and a quantitative analysis of these species are important for a deep understanding of the photodegradation mechanism. For a thorough comparison, the MOF samples were treated under different conditions: (a) freshly prepared CuTz-1; (b) CuTz-1 pretreated by H_2O_2; (c) CuTz-1 pretreated under irradiation of Xe lamp; (d) CuTz-1 pretreated by H_2O_2 under irradiation of Xe lamp; (e) CuTz-1 after one cycle of the degradation of MO; (f) CuTz-1 after 4 cycles of the degradation of MO (Figure S22).

As depicted in Figure 8a, the deconvoluted Cu 2p XPS data provided solid spectroscopic evidence that the Cu atoms are almost entirely in +1 valence in the pristine CuTz-1, which is characterized by the $2p_{3/2}$ peak at ~ 933 eV. The weak satellite at *ca*. 940 eV may imply the presence of a tiny amount of Cu^{II} species. CuTz-1 seems to be resistant to the oxidation of H_2O_2 and remains stable under the Xe lamp irradiation, since the signal at 940 eV is practically unchanged in intensity after the treatment of CuTz-1 with H_2O_2 or under photo-irradiation, revealing that no additional Cu^{II} was formed (Figure 8b, c). Interestingly, when both H_2O_2 and irradiation were applied to CuTz-1, a small amount of Cu^{II} was formed, as evidenced by the appearance of an additional weak Cu $2p_{3/2}$ signal at 934.7 eV together with the typical shake-up satellites between 938 - 947 eV (8.5%, Figure 8d). Furthermore, the content of Cu^{II} continued to increase when CuTz-1 was used as photocatalyst in the degradation of dyes; it reached to 14.7% and 18.8% after one and four reaction cycles, respectively (Figure 8e and f).

The presence of O-containing species and BF_4^- counterions was also identified by the O1s peak at 531.5 eV and the F1s peak at 685.0 eV (see Figure S23). In addition, the O1s binding energy at 531.5 eV is characteristic for hydroxyl (OH^-) species. A quantitative analysis of the O1s and F1s XPS results allowed to obtain more information about the relative concentration of O and F species on the surface of CuTz-1 under various experimental conditions. Overall, the surficial content of O remained rising with the proceeding of the catalytic reaction, while the F content kept dropping.

Based on the results of the XPS study, Cu^{II} ions are assumed to be created upon irradiation on CuTz-1 in the presence of H_2O_2. The photo-induced Cu^{II} may combine with O-

containing ligands (predominantly OH^-) to form Cu^{II}-O(H) species on the surface of MOF. Degradation of dyes seems to be more in favor of the formation of such surficial Cu^{II}-O(H) compounds. The continuous decrease in surficial F content may be attributed to the replacement of BF_4^- by O-containing anions (OH^-).

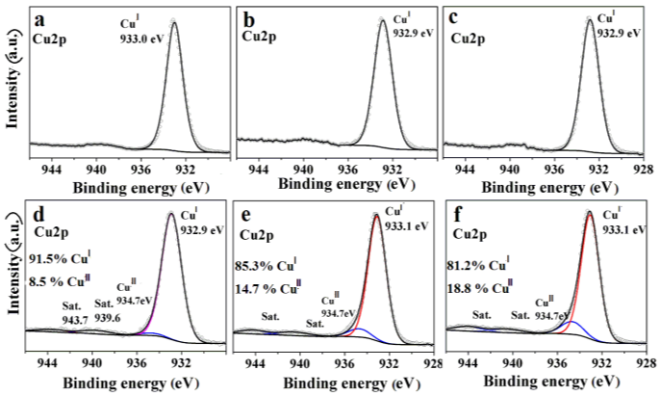

Figure 8. Cu 2p region of the deconvoluted XPS for six samples (a) freshly prepared CuTz-1; (b) CuTz-1 pretreated by H_2O_2; (c) CuTz-1 pretreated under irradiation of Xe lamp; (d) CuTz-1 pretreated by H_2O_2 under irradiation of Xe lamp; (e) CuTz-1 after one cycle of the degradation of MO; (f) CuTz-1 after 4 cycles of the degradation of MO. The formation of Cu^{II} species was also confirmed by their characteristic satellite peaks between 938-947 eV (MO: methyl orange).

Effect of the presence of •OH scavenger – TBA

Our experimental results showed that the addition of H_2O_2 is necessary to achieve a high efficiency of the photocatalytic degradation over CuTz-1. As generally accepted, hydroxyl radicals (•OH) are the active species in the H_2O_2-involved photocatalytic reactions over MOFs.[71, 74] To verify the major active species in our system, *tert*-butyl alcohol (TBA) was used as a scavenger of hydroxyl radicals in the degradation reaction.[35, 75, 76] As illustrated in Figure 9, the addition of TBA greatly depressed the photocatalytic efficiency for the degradation of RhB. In the presence of 100 μL (or 200 μL) of TBA, 70.2% (or 64.2%) of RhB was degraded after 22 min, and the first-order reaction rate constant dropped to only *ca* 1/4 of the original value (0.190 min^{-1} *vs*. 0.056 (or 0.044) min^{-1}). It is therefore concluded that the major active species may be •OH for the present system, the degradation performance would thus heavily rely on the efficiency of generating •OH during the reaction.

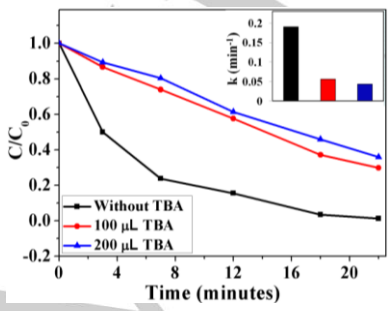

Figure 9. Photocatalytic degradation of RhB over CuTz-1 with or without TBA; inset: comparison of the apparent reaction rate constants in the presence/absence of TBA (black: without TBA, red: 100 μL TBA, blue: 200 μL TBA, RhB: rhodamine B, TBA: *tert*-butyl alcohol).

Proposed mechanism

Based on our research results, we propose a possible mechanism to account for the observed high efficient photocatalytic degradation of dyes. Illumination of CuTz-1 by photons with energy equal to or greater than its band gap excites electrons (e^-) from the valence band (VB) to the conduction band (CB) and leaving holes (h^+) in VB. These holes are possibly located at the metal ions, that is, they are present as Cu^{II} ions in the framework of CuTz-1.[77] This hypothesis seems to be consistent with the assignment of the luminescence peak at 525 nm of CuTz-1, which is attributed to a ^{3}MLCT excited state. Although a widely accepted viewpoint is that the organic linker is regarded as VB and the metallic cluster plays the role of CB for MOF-based semiconductors,[55, 78] for the present case the situation is probably reversed: Cu ions or Cu_5tz_6 clusters possibly act as VB, while triazole ligands as CB. For those already extensively studied MOF-based semiconductors, the metal ions are either in their higher valence (*e.g.* Fe^{III} in MIL-53(Fe), Zr^{IV} in UiO-66)[30, 34, 79-82] or in very stable valence (*e.g.* Zn^{II} in MOF-5),[83, 84] and therefore it is very difficult for these metal ions to lose electrons. For the present case, CuTz-1 contains only Cu^{I} clusters in the framework and Cu^{I} can be easily transformed to Cu^{II}, as indicated by the standard electrochemical potential of Cu^{II}/Cu^{I} (0.159 V). Our hypothesis is fully supported by the XPS observation that Cu^{II} ions appeared and increased in concentration when irradiating CuTz-1 in the presence of H_2O_2 (and dyes).

The photo-induced electrons and holes are easily recombined, therefore no Cu^{II} can be detected on the surface of CuTz-1 after irradiation under Xe-lamp in the absence of H_2O_2 and dyes, as verified by XPS analysis (Figure 8c).

When H_2O_2, an efficient electron scavenger, was added, it can combine with an electron to produce •OH and OH^- (equation 2). Furthermore, photogenerated holes (Cu^{II}) can be stabilized within the framework of CuTz-1 through bonding with hydroxides (generated from equation 2) and/or other O-containing species in the reaction system. The presence of Cu^{II}-O(H) species on the surface of catalyst was verified by XPS analysis for irradiated samples in the presence of H_2O_2 (Figure 8d). About 8.5% surficial Cu atoms were identified to be in the oxidation state +2 for this sample.

The *in-situ* formed Cu^{II} species can undergo Fenton-like reactions to produce •OH, as shown in equations. 3-a and 3-b. When dyes were added to the photocatalytic system, degradation of dyes consumes •OH, which seems to promote the reactions of equations. 1, 2 and 3 and accelerate the formation of Cu^{II} and hydroxyl (OH^-) species, in accordance with the XPS analysis on the samples after 1 or 4 cycles of dye degradation (see Figure 8e, f and Figure S23e, f).

The Cu^{II}-O(H) species are considered to exist only on the surface of CuTz-1. The presence of Cu^{II} on the surface, as determined by XPS, cannot be applied automatically to the inner part of CuTz-1, since XPS is a surface analysis technique. The PXRD patterns of CuTz-1 after several cycles of dye-degradation remained almost identical to that of pristine MOF. If more than 10% of total Cu atoms in the MOF were in oxidation state of +2, the structure of CuTz-1 would experience a remarkable change, which is obviously not true for the present case. In our previous paper, we already showed that hydroxide ions fail to enter the channels of the MOF by anion-exchange,[42] because anions with higher hydration energy (OH^-) would be

energetically unfavorable to replace anions of lower hydration energy (NO_3^-, BF_4^-) located within the frames of the MOF. The same argument can be applied to the present case, that is, it would be rather difficult for hydroxides (or other smaller-sized, highly charged O-containing anions) to enter the channels of CuTz-1 *via* anion-exchange. The photogenerated Cu^{II} inside of the MOF would not be stabilized by OH^- and probably be transformed back to Cu^I quickly.

As revealed above, the hydroxyl radical (•OH) as active species plays a key role in the degradation of organic dyes, which is also verified and widely accepted by the academic community. For MOF-based semiconductors, the photogenerated holes are not very effective in producing •OH and thus the pristine MOFs usually show a moderate photocatalytic activity towards organics.[30] In some recent reports, this drawback has been (at least partially) overcome by forming composites with other types of materials.[85-88] In this work, we demonstrate that CuTz-1 can generate •OH under irradiation and in the presence of H_2O_2 through two pathways, as shown in equations. 2 and 3. Consequently, CuTz-1 is highly efficient in producing •OH and achieved a superior photocatalytic activity towards dyes. It should be mentioned here that one of the advantages of Cu-based Fenton-like catalysts is that they can be used in neutral solution, just as shown in Table S3, which recorded the pH values of the reaction solution before and after the degradation of dyes.[82]

The proposed main photocatalytic mechanism is illustrated in Figure 10. Other mechanisms are also possible, such as (1) homolytic cleavage of H_2O_2 under irradiation; (2) Oxidation of the surficial Cu^I to Cu^{II} by H_2O_2, and thus facilitating a Fenton-like reaction; (3) involvement of O_2 from air, which are believed to be less efficient as compared to the proposed mechanism (equations. 1-3), and may account for the lower removal rates of dyes when the degradation was conducted in the dark or without H_2O_2.

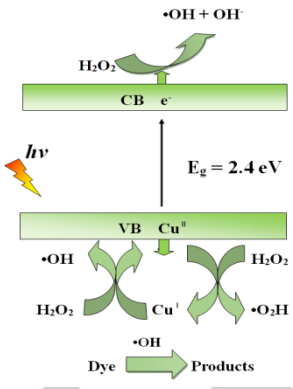

Figure 10. Proposed mechanism of the photocatalytic degradation over CuTz-1.

$$CuTz\text{-}1 + h\nu \rightarrow CuTz\text{-}1\ [e^- + h^+(Cu^{II})] \quad (1)$$
$$H_2O_2 + e^- \rightarrow \bullet OH + OH^- \quad (2)$$
$$Cu^{II} + H_2O_2 \rightarrow Cu^I + \bullet O_2H + H^+ \quad (3\text{-}a)$$
$$Cu^I + H_2O_2 \rightarrow \bullet OH + OH^- + Cu^{II} \quad (3\text{-}b)$$

Product analysis of photocatalytic degradation of dyes

The final products and intermediates generated during the degradation process were analyzed by LC/MS and by interpretation of their fragment ions in the mass spectra. The supernatants of the dye solutions (MLB, RhB, MO and MB) at different degradation times were taken for mass spectrometry detection, and their MS patterns are shown in Figure S24-S27. Based on MS measurements, the main metabolites resulting from degradation of dyes were deduced and logically reported according to their molecular weight (Scheme S1-S4), which indicates that the present catalytic system can effectively degrade or decompose the dyes under investigation.

Conclusions

A novel MOF (CuTz-1) was successfully constructed from Cu^I and 3,5-diphenyltriazolate, extensively characterized by SXRD, PXRD, IR, UV-vis DRS, TGA, emission spectra, SEM and XPS. CuTz-1, isostructural to our previously reported AgTz-1, features an unprecedented Cu_5tz_6 cluster as SBU in the 3D polymeric structure and a porous cationic framework with *ca* 0.83 nm diameter channels along the crystallographic *c*-axis. In stark contrast to its silver analog, CuTz-1 exhibits semiconductor-like behavior and high efficiency in photocatalytic degradation of dyes of various structural types (cationic, anionic, azo-type and triarylmethane type) in the presence of H_2O_2. It has been suggested that photo-irradiation in the presence of H_2O_2 leads to the formation of Cu^{II} species as the photogenerated holes that are stabilized by O-containing species (predominantly OH^-), as evidenced by the XPS results. The superior photocatalytic performance of CuTz-1 is ascribed to two effective pathways to produce potent oxidant – •OH: (1) H_2O_2 scavenges a photogenerated electron to produce •OH; (2) a Fenton-like Cu^I/Cu^{II} redox reaction can also efficiently generate •OH. It has to be pointed out that a dye-mixture (MLB, MO, RhB, MB) was totally decolorized by using CuTz-1 and H_2O_2 under a Xe lamp or *natural sunlight*. The superior properties of CuTz-1, such as high efficiency (comparable to those of composites), wide applicability (4 different types of dyes under investigation), economic feasibility (facile and large-scale preparation), simple operation and reusability, make it a kind of heterogeneous photocatalyst with potential practical value for the treatment of dye-containing wastewater. Future studies are underway on the modification of the MOF catalysts to achieve an even higher catalytic activity and we also foresee the application of CuTz-1 and its analogs to other important catalytic reactions.

Acknowledgements

This work has been supported in China by the National Natural Science Foundation of China (Grant No. 21471132) and in USA by NSF-CREST Center for Innovation, Research and Education in Environmental Nanotechnology (CIRE2N) (Grant Number HRD-1736093) and NASA (Grant 17-EPSCoRProp-0032). P. Guo acknowledges the funding from the European Union's Horizon 2020 research and innovation program under the Marie Sklodowska-Curie grant agreement No. 641887.

Keywords: Metal-organic framework • Semiconductor • Photocatalyst • Fenton-like reaction • Dye degradation

[1] S. Arslan, M. Eyvaz, E. Gürbulak, E. Yüksel, A Review of State-of-the-Art Technologies in Dye-Containing Wastewater Treatment - The Textile Industry Case, **2016**, InTech. Available from: http://www.intechopen.com/books/textile-wastewater -treatment.

[2] Z. Wang, M. Xue, K. Huang, Z. Liu, Textile Dyeing Wastewater Treatme nt, **2011**, InTech. Available from: http://www.intechopen.com/books/advances-in-treating-textile-effluent/textile-dyeing-wastewater-treatment.
[3] T. Robinson, G. McMullan, R. Marchant, P. Nigam, *Bioresource Technol.* **2001**, *77*, 247-255.
[4] Q. Chen, Q. He, M. Lv, Y. Xu, H. Yang, X. Liu, F. Wei, *Appl. Surf. Sci.* **2015**, *327*, 77-85.
[5] M. B. Ahmed, J. L. Zhou, H. H. Ngo, W. Guo, N. S. Thomaidis, J. Xu, *J. Hazard. Mater.* **2017**, *323*, 274-298.
[6] Y.-C. Hsu, C.-H. Yen, H.-C. Huang, *J. Chem. Technol. Biotechnol.* **1998**, *71*, 71-76.
[7] A. K. Verma, R. R. Dash, P. Bhunia, *J. Environ. Manage.* **2012**, *93*, 154-168.
[8] K. N. Oviedo, D. S. Aga, *J. Hazard. Mater.* **2016**, *316*, 242-251.
[9] C. S. Diercks, Y. Liu, K. E. Cordova, O. M. Yaghi, *Nature Mater.* **2018**, *17*, 301-307.
[10] P. Kumar, A. Pournara, K.-H. Kim, V. Bansal, S. Rapti, M. J. Manos, *Prog. Mater. Sci.* **2017**, *86*, 25-74.
[11] H. Li, K. Wang, Y. Sun, C. T. Lollar, J. Li, H.-C. Zhou, *Mater. Today* **2018**, *21*, 108-121.
[12] M. Wen, K. Mori, Y. Kuwahara, T. An, H. Yamashita, *Appl. Catal. B Environ.* **2017**, *218*, 555-569.
[13] J. Li, X. Wang, G. Zhao, C. L. Chen, Z. Chai, *Chem. Soc. Rev.* **2018**, *47*, 2322-2356.
[14] D. Britt, D. Tranchemontagne, O. M. Yaghi, *Proc. Natl. Acad. Sci. USA* **2008**, *105*, 11623-11627.
[15] H. Li, M. Eddaoudi, M. O'Keeffe, O. M. Yaghi, *Nature* **1999**, *402*, 276-279.
[16] J. Rowsell, O. M. Yaghi, *Microporous Mesoporous Mat.* **2004**, *73*, 3-14.
[17] M. Rafatullah, O. Sulaiman, R. Hashim, A. Ahmad, *J. Hazard. Mater.* **2010**, *177*, 70-80.
[18] S. Chen, J. Zhang, C. Zhang, Q. Yue, Y. Li, C. Li, *Desalination* **2010**, *252,* 149-156.
[19] L.-L. Lv, J. Yang, H.-M. Zhang, Y.-Y. Liu, J.-F. Ma, *Inorg. Chem.* **2015**, *54*, 1744-01755.
[20] X. Zhao, X.-H. Bu, T. Wu, S.-T. Zheng, L. Wang, P.-Y. Feng, *Nat. Commun.* **2013**, *4*, 2344-2312.
[21] M. Plabst, L. B. McCusker, T. Bein, *J. Am. Chem. Soc.* **2009**, *131*, 18112-18118.
[22] E. Haquea, J. E. Lee, I. T. Jang, Y. K. Hwang, J.-S. Chang, J. Jegal, S. H. Jhung, *J. Hazard. Mater.* **2010**, *181*, 535-542.
[23] M. N. Chong, B. Jin, C. W. K. Chow, C. Saint, *Water Res.* **2010**, *44*, 2997-3027.
[24] J. Kou, C. Lu, J. Wang, Y. Chen, Z. Xu, R. S. Varma, *Chem. Rev.* **2017**, *117*, 1445-1514.
[25] S. N. Habisreutinger, L. Schmidt-Mende, J. K. Stolarczyk, *Angew. Chem.* **2013**, *52*, 7372 - 7408.
[26] N. Stock, J. Peller, K. Vinodgopal, P. V. Kamat, *Sci. Technol.* **2000**, *34*, 1747-1750.
[27] H. Lachheb, E. Puzenat, A. Houas, M. Ksibi, E. Elaloui, C. Guillard, J.-M. Herrmann, *Appl. Catal. B Environ.* **2002**, *39*, 75-90.
[28] Y. Zheng, L. Zheng, Y. Zhan, X. Lin, Q. Zheng, K. Wei, *Inorg. Chem.*, **2007**, *46*, 6980-6986.
[29] M. Sharma, T. Jain, S. Singh, O. P. Pandey, *Solar Energy* **2012**, *86*, 626-633.
[30] J. Qiu, X. Zhang, Y. Feng, X. Zhang, H. Wang, J. Yao, *Appl. Catal. B Environ.* **2018**, *231*, 317-342.
[31] X. L. X. Francesc, A. Corma, H. Garcia, *J. Phys. Chem. C* **2007**, *111*, 80-85.
[32] P. Mahata, G. Madras, S. Natarajan, *J. Phys. Chem. B* **2006**, *110*, 13759-13768.
[33] J. Gascon, M. D. Hernández-Alonso, A. R. Almeida, G. P. M. van Klink, F. Kapteijn, G. Mul, *ChemSusChem.* **2008**, *1*, 981-983.
[34] J.-J. Du, Y.-P. Yuan, J.-X. Sun, F.-M. Peng, X. Jiang, L.-G. Qiu, A.-J. Xie, Y.-H. Shen, J.-F. Zhu, *J. Hazard. Mater.* **2011**, *190*, 945-951.
[35] H. Zhao, Q. Xia, H. Xing, D. Chen, H. Wang, *ACS Sustainable Chem. Eng.* **2017**, *5*, 4449-4456.
[36] C. Racles, M.-F. Zaltariov, M. Iacob, M. Silion, M. Avadanei, *Appl. Catal. B Environ.* **2017**, *205*, 78-92.
[37] Y. Fu, D. Sun, Y. Chen, R. Huang, Z. Ding, X. Fu, Z. Li, *Angew. Chem. Int. Ed.* **2012**, *51*, 3364-3367.
[38] M. W. Logan, S. Ayad, J. D. Adamson, T. Dilbeck, H. B. Kenneth, F. J. Uribe-Romo, *J. Mater. Chem. A* **2017**, *5*, 11854-11863.
[39] H. Wang, X. Yuan, Y. Wu, G. Zeng, X. Chen, L. Leng, Z. Wu, L. Jiang, H. Li, *J. Hazard. Mater.* **2015**, *286*, 187-194.
[40] G. Yang, R. G. Raptis, *Chem. Commun.* **2004**, 2058-2059.
[41] G. Yang, J. A. Santana, M. E. Rivera-Ramos, O. Garcia-Ricard, J. J. Saavedra-Arias, Y. Ishikawa, A. J. Hernández-Maldonado, R. G. Raptis, *Microporous Mesoporous Mat*. **2014**, *183*, 62-68.
[42] L.-L. Li, X.-Q. Feng, R.-P. Han, S.-Q. Zang, G. Yang, *J. Hazard. Mater.* **2017**, *321*, 622-628.
[43] M. O'Keeffe, O. M. Yaghi, *Chem. Rev.* **2012**, *112*, 675-702.
[44] P. Pyykkö, *Chem. Rev.* **1997**, *97*, 597-636.
[45] J. Fritzsche, M. Grzywa, D. Denysenko, V. Bon, I. Senkovska, S. Kaskelb, D. Volkmer, *Dalton Trans.* **2017**, *46*, 6745-6755.
[46] T. Wen, D.-X. Zhang, J. Liu, R. Lin. J. Zhang, *Chem. Commun.* **2013**, *49*, 5660-5662.
[47] H. V. Rasika Dias, H. V. K. Diyabalanage, M. G. Eldabaja, O. Elbjeirami, M. A. Rawashdeh-Omary, M. A. Omary, *J. Am. Chem. Soc.* **2005**, *127*, 7489-7501.
[48] T. Wen, X.-P. Zhou, D.-X. Zhang, D. Li, *Chem. Eur. J.* **2014**, *20*, 644-648.
[49] J.-H. Wang, M. Li, J. Zheng, X.-C. Huang, D. Li, *Chem. Commun.* **2014**, *50*, 9115-9118.
[50] H. V. Rasika Dias, H. V. K. Diyabalanage, M. A. Rawashdeh-Omary, M. A. Franzman, M. A. Omary, *J. Am. Chem. Soc.* **2003**, *125*, 12072-12073.
[51] T. Wen, D.-X. Zhang, J. Zhang, *Inorg. Chem.* **2013**, *52*, 12-14.
[52] K. S. W. Sing, D. H. Everett, R. A. W. Haul, L. Moscou, R. A. Pierotti. J. Rouquerol, T. Siemieniewska, *Pure Appl. Chem.* **1985**, *57*, 603-619.
[53] J. Zhao, W.-W. Dong, Y.-P. Wu, Y.-N. Wang, C. Wang, D.-S. Li, Q.-C. Zhang, *J. Mater. Chem. A* **2015**, *3*, 6962-6969.
[54] Q. Liang, M. Zhang, Z.. Zhang, C. Liu, S. Xu, Z. Li, *J. Alloy. Compd.* **2017**, *690*, 123-130.
[55] X. Li, Y. Pi, L. Wu, Q. Xia, J. Wu, Z. Li, J. Xiao, *Appl. Catal. B Environ.* **2017**, *202*, 653-663.
[56] B. K. Ghosh, S. Hazra, B. Naik, N. N. Ghosh, *Powder Technol.* **2015**, *269*, 371-378.
[57] P. K. Sahoo, D. Thakur, D. Bahadura, B. Panigrahy, *RSC Adv.* **2016**, *6*, 106723-106731.
[58] C. Zhang, L. Ai, J. Jiang, *J. Mater. Chem. A* **2015**, *3*, 3074-3081.
[59] H. Wang, J. Shen, Y. Li, Z. Wei, G. Cao, Z. Gai, K. Hong, P. Banerjee, S. Zhou, *ACS Appl. Mater. Interfaces* **2013**, *5*, 9446-9453.
[60] Z. Wang, C. Chen, F. Wu, B. Zou, M. Zhao, J. Wang, C. Feng, *J. Hazard. Mater.* **2009**, *164*, 615-620.
[61] M. R. Kim, D. K. Lee, D. J. Jang, *Appl. Catal. B* **2011**, *103*, 253-260.
[62] H. Chen, K. Shen, J. Chen, X. Chen, Y. Li, *J. Mater. Chem. A* **2017**, *5*, 9937-9945.
[63] N. Gupta, H. M. Singh, R. K. Sharma, *J. Mol. Catal. A Chem.* **2011**, *335*, 248-252.
[64] L. Shi, T. Wang, H. Zhang, K. Chang, X. Meng, H. Liu, J. Ye, *Adv. Sci.* **2015**, *2*, 1-8.
[65] G.-H. Cui, C.-H. He, C.-H. Jiao, J.-C. Geng, V. A. Blatov, *CrystEngComm* **2012**, *14*, 4210-4216.
[66] J. I. Pankove, *Optical Processes in Semiconductors*, *Prentice Hall*, **1971**.
[67] W. M. Wesley, W. G. H. Harry, *Reflectance Spectroscopy*, *Wiley*, **1966**.
[68] R. Gagné, C. Koval, T. Smith, M. Cimolino, *J. Am. Chem. Soc.* **1979**, *101,* 4571-4580.
[69] P. Jones, J. Jeffery, J. Maher, J. McCleverty, P. Rieger, M. Ward, *Inorg. Chem.* **1997,** *36,* 3088-3095.
[70] D. D'Alessandro, F. Richard Keene, *Chem. Rev.* **2006**, *106*, 2270-2298.
[71] C.-C. Wang, J.-R. Li, X.-L. Lv, Y.-Q. Zhang, G. Guo, *Energy Environ. Sci.* **2014**, *7*, 2831-2867.
[72] Z. Wu, X. Yuan, J. Zhang, H. Wang, L. Jiang, G. Zeng, ChemCatChem **2017**, *9*, 41-64.
[73] J. Zhao, W.-W. Dong, Y.-P. Wu, Y.-N. Wang, C. Wang, D.-S. Li, Q.-C. Zhang, *J. Mater. Chem. A* **2015**, *3*, 6962-6969.
[74] F. Wang, Z. S. Liu, H. Yang, Y. X. Tan, J. Zhang, *Angew. Chem. Int. Ed.* **2011**, *50*, 450-453.
[75] R. Liang, F. Jing, L. Shen, N. Qin, L. Wu, *Nano Res.* **2015**, *8*, 3237-3249.

[76] C. Zhang, L. Ai, J. Jiang, *Ind. Eng. Chem. Res.* **2015**, *54*, 153-163.
[77] Z.-L. Wu, C.-H. Wang, B. Zhao, J. Dong, F. Lu, W.-H. Wang, W.-C. Wang, G.-J. Wu, J.-Z. Cui, P. Cheng, *Angew. Chem. Int. Ed.* **2016**, *55*, 4938 -4942.
[78] L. Shi, T. Wang, H. Zhang, K. Chang, X. Meng, H. Liu, J. Ye, *Adv. Sci.* **2015**, *2*, 1-8.
[79] F. X. Llabrés i Xamena, A. Corma, H. Garcia, *J. Phys. Chem. C* **2007**, *111*, 80-85.
[80] L. Shen, S. Liang, W. Wu, R. Liang, L. Wu, *J. Mater. Chem. A* **2013**, *1*, 11473-11482.
[81] J. He, J. Wang, Y. Chen, J. Zhang, D. Duan, Y. Wang, Z. Yan, *Chem. Commun.* **2014**, *50*, 7063-7066.
[82] A. D. Bokare, W. Y. Choi, *J. Hazard. Mater.* **2014**, *275*, 121-135.
[83] M. Alvaro, E. Carbonell, B. Ferrer, F. X. Llabrés i Xamena, H. Garcia, *Chem-Eur. J.* **2007**, *13*, 5106-5112.
[84] T. Tachikawa, J. R. Choi, M. Fujitsuka, T. Majima, *J. Phys. Chem. C* **2008**, *112*, 14090-14101.
[85] S. Gao, T. Feng, C. Feng, N. Shang, C. Wang, *J. Colloid Interface Sci.* **2016**, *466*, 284-290.
[86] H. Wang, F.-X. Yin, B.-H. Chen, X.-B. He, P.-L. Lv, C.-Y. Ye, D.-J. Liu, *Appl. Catal. B Environ.* **2017**, *205*, 55-67.
[87] C. Zhang, L. Ai, J. Jiang, *Ind. Eng. Chem. Res.* **2015**, *54*, 153-163.
[88] Y. Feng, H. Lu, X. Gu, J. Qiu, M. Jia, C. Huang, J. Yao, *J. Phys. Chem. Solids* **2017**, *102*, 110-114.

Entry for the Table of Contents

Layout 1:

FULL PAPER

A thermally and chemically stable Cu^{I} triazolate MOF (CuTz-1) has been prepared and demonstrated to exhibit high photocatalytic activity towards degradation of dyes in the presence of H_2O_2. CuTz-1 can be used as a catalyst at least 4 cycles without significant change of the crystallinity and catalytic activity. Shown here are the photos taken before and after degradation of a dye-mixture under *natural sunlight* by using CuTz-1 as photocatalyst (mixed dyes: methyl orange, methyl blue, methylene blue and rhodamine B).

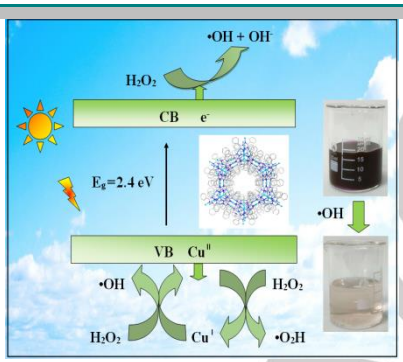

*Chen-Xia Liu,[a] Wen-Hua Zhang,[a] Nan Wang,[a] Penghu Guo,[b] Martin Muhler,[b, c] Yuemin Wang,[d] Shiru Lin,[e] Zhongfang Chen,[e] Guang Yang * [a]*

Page No. – Page No.

Highly efficient photocatalytic degradation of dyes by a novel copper-triazolate metal-organic framework